Nonequilibrium Solvation Effects for a Polyatomic Reaction in Solution

Yao-Yuan Chuang and Donald G. Truhlar*

Contribution from the Department of Chemistry and Supercomputer Institute, University of Minnesota, Minneapolis, Minnesota 55455-0431

Received June 1, 1999

Abstract: We present a general linear-response method for including nonequilibrium solvation effects (solvent friction effects) in variational transition state theory with multidimensional tunneling (VTST/MT) for calculating reaction rate constants in solution. The generalized Langevin approach is used to include a collective solvent coordinate into VTST/MT, and a general prescription is suggested for coupling this collective solvent coordinate to the solute, which is treated in its full dimensionality. The new formalism is illustrated by application to the aqueous free radical reaction $H + CH_3OH \rightarrow H_2 + CH_2OH$ at 298 K. This reaction is treated with a linear mixing of Hartree−Fock theory and Austin Model 1 with specific reaction parameters (HF||AM1-SRP). The results with nonequilibrium solvation (NES) are compared to those obtained earlier with the separable equilibrium solvation (SES) and the equilibrium solvation path (ESP) approximations. We focus on the speedup due to solvation and on the kinetic isotope effects (KIEs). We calculate that nonequilibrium solvation decreases the rate constant by a factor of 2 but changes the KIEs by less than 2%. We also present results that show how the nonequilibrium effect depends on the solvation time and the strength of the solute−solvent coupling.

1. Introduction

We have recently presented[1−3] general procedures for calculating reaction rates in solution by variational transition state theory with multidimensional tunneling[4−6] (VTST/MT) under the assumption of an equilibrium solvation path (ESP) or the simpler assumption of separable equilibrium solvation (SES). We illustrated these methods in ref 2 for two ionic reactions, and in a subsequent paper[3] we applied them to the free radical reaction

$$H + CH_3OH \rightarrow H_2 + CH_2OH \qquad (R1)$$

in aqueous solution.

The present paper extends these methods to include the effect of nonequilibrium solvation (NES) on reaction rates, a subject that has received considerable attention in recent years.[7] The present extension builds on methods presented previously in a number of papers,[8−13] and it provides a systematic framework for treating arbitrary systems including all degrees of freedom of the solute.

Central to the hierarchy of methods employed in this work is the division of the system into an explicit subspace and an implicit bath. In general, for an *N*-atom solute, one can calculate equilibrium solvation (ES) rate constants (either SES or ESP) by treating the 3*N* solute coordinates explicitly and taking all of the solvent coordinates as implicit.[2,3,12,14−16] This requires the potential of mean force[17] $W(\mathbf{x})$ in the 3*N*-dimensional space $\mathbf{x}$ of solute coordinates. From a dynamical perspective, this treatment can include full solute anharmonicity and nonlinear solute−solvent coupling, although in practical work one might use local harmonic approximations for the solute or assume linear response of the solvent at various stages of an actual calculation.

To introduce NES effects one must dynamically determine the extent and nature of solvent participation in the reaction coordinate.[18,19] One can do this by selecting *m* solvent coordi-

(1) Truhlar, D. G.; Liu, Y.-P.; Schenter, G. K.; Garrett, B. C. *J. Phys. Chem.* **1994**, *98*, 8396.
(2) Chuang, Y.-Y.; Cramer, C. J.; Truhlar, D. G. *Int. J. Quantum Chem.* **1998**, *70*, 887.
(3) Chuang, Y.-Y.; Radhakrishnan, M.; Fast, P.; Cramer, C. J.; Truhlar, D. G. *J. Phys. Chem.* **1999**, *103*, 4893.
(4) Truhlar, B. G.; Isaacson, A. D.; Garrett, B. C. In *Theory of Chemical Reaction Dynamics*; Baer, M., Ed.; CRC Press: Boca Raton, FL,1985; Vol. 4, p 65.
(5) Truhlar, D. G.; Garrett, B. C. *Annu. Rev. Phys. Chem.* **1984**, *35*, 159.
(6) Lu-D.-h.; Truong, T. N.; Melissas, V. S.; Lynch, G. C.; Liu, Y.-P.; Garrett, B. C.; Steckler, R.; Isaacson, A. D.; Rai, S. N.; Hancock, G. C.; Lauderdale, J. G.; Joseph, T.; Truhlar, D. G. *Comput. Phys. Commun.* **1997**, *71*, 235.
(7) For reviews, see: (a) Truhlar, D. G.; Hase, W. L.; Hynes, J. T. *J. Phys. Chem.* **1983**, *87*, 2664, 5523(E). (b) Truhlar, D. G.; Garrett, B. C.; Klippenstein, S. J. *J. Phys. Chem.* **1996**, *100*, 12771. (c) Bianco, R.; Hynes, J. T. In *Solvent Effects and Chemical Reactivity*; Tapia, O., Bertrán, J., Eds.; Kluwer: Dordrecht, The Netherlands,1980; p 259. (d) Cramer, C. J.; Truhlar, D. G. *Chem. Rev.*, **1999**, *99*, 2161.
(8) Lee, S.; Hynes, J. T. *J. Chem. Phys.* **1988**, *88*, 6853.
(9) Pollak, E.; Tucker, S. C.; Berne, B. J. *Phys. Rev. Lett.* **1990**, *65*, 1399.
(10) Schenter, G. K.; McRae, R. P.; Garrett, B. C. *J. Chem. Phys.* **1992**, *97*, 9116.
(11) Truhlar, D. G.; Schenter, G. K.; Garrett, B. C. *J. Chem. Phys.* **1993**, *98*, 5756.
(12) Garrett, B. C.; Schenter, G. K. *Int. Rev. Phys. Chem.* **1994**, *13*, 263.
(13) Garrett, B. C.; Schenter, G. K. In *Structure and Reactivity in Aqueous Solution*; Cramer, C. J., Truhlar, D. G., Eds.; ACS Symposium Series 568; American Chemical Society: Washington, DC, 1994, p 122.
(14) Chandler, D. *J. Chem. Phys.* **1978**, *68*, 2959.
(15) Kreevoy, M. M.; Truhlar, D. G. In *Investigation of Rates and Mechanisms of Reactions*; Bernasconi, C. F., Ed.; *Techniques of Chemistry; Volume* 4th ed.; Wiley & Sons: New York, 1986; Vol. 6, Part I, p 13.
(16) Tucker, S. C. In *New Trends in Kramers' Rate Theory*; Talkner, P., Hänggi, P., Eds.; Kluwer: Dordrecht, 1995; p 5.
(17) See, e.g.: King, P. M. In *Computer Simulation of Biomolecular Systems*; van Gunsteren, W. F., Weiner, P. K., Wilkinson, A. J., Eds.; ESCOM: Leiden, 1993; Vol. 2, p 267.
(18) (a) Gertner, B. J.; Bergsma, J. P.; Wilson, K. R.; Lee, S.; Hynes, J. T. *J. Chem. Phys.* **1987**, *86*, 1377. (b) Kim, H. J.; Hynes, J. T. *J. Am. Chem. Soc.* **1992**, *114*, 10528.

10.1021/ja991809i CCC: $18.00
Published on Web 10/13/1999

nates on a physical basis; these solvent coordinates may be Cartesian coordinates of individual solvent atoms, but, to be realistic, such an approach often requires very large m. Thus, it is often preferable to use one or more collective solvent coordinates, e.g., a coordinate representing the solvent electric polarization field.[8,11,20−23] Provided one can calculate the correct potential of mean force $w(\mathbf{x}, \mathbf{y})$, where $\mathbf{x}$ denotes the solute coordinates, and $\mathbf{y}$ denotes the set of m selected solvent coordinates, such a treatment can be exact if all implicit solvent coordinates (the orthogonal complement of $\mathbf{y}$ in the full set of solvent coordinates) are at equilibrium, and, in a classical world, it can provide a variational transition state upper bound even if they are not.[16] This observation provides one possible starting point for a variational transition state theory of reactions in solution that includes nonequilibrium solvation.

In the present paper we restrict ourselves to $m = 1$, so that $\mathbf{y}$ reduces to a scalar variable y. Furthermore we write

$$w(\mathbf{x}, y) = W(\mathbf{x}) + \Delta G^0_{\mathrm{NES}}(\mathbf{x}, y) \quad (1)$$

where $W(\mathbf{x})$ is the usual potential of mean force for solute only,[17] and $\Delta G^0_{\mathrm{NES}}(\mathbf{x}, y)$ is the nonequilibrium contribution to the standard-state free energy of solvation. We may also write[2]

$$W(\mathbf{x}) = V(\mathbf{x}) + \Delta G^0_{\mathrm{S}}(\mathbf{x}) \quad (2)$$

where $V(\mathbf{x})$ is the gas-phase potential energy surface, and $\Delta G^0_{\mathrm{S}}(\mathbf{x})$ is a free energy of solvation for constrained values $\mathbf{x}$ of the solute coordinates. Then, if desired, we can regroup the terms as

$$w(\mathbf{x}, y) = V(\mathbf{x}) + \Delta G^0_{\mathrm{NE}}(\mathbf{x}, y) \quad (3)$$

where

$$\Delta G^0_{\mathrm{NE}}(\mathbf{x}, y) = \Delta G^0_{\mathrm{S}}(\mathbf{x}) + G_{\mathrm{NES}}(\mathbf{x}, y) \quad (4)$$

and $\Delta G^0_{\mathrm{NE}}(\mathbf{x})$ denotes the standard-state nonequilibrium free energy of solvation. The equilibrium term $\Delta G^0_{\mathrm{S}}(\mathbf{x})$ is calculated by an SM5-class solvation model,[24−27] which includes a linear-response treatment of electrostatics[28] and a general (nonlinear) treatment of first-solvation-shell effects,[29] and the nonequilibrium term $G_{\mathrm{NES}}(\mathbf{x}, y)$ is modeled using linear response (LR) based on the generalized Langevin equation with m collective solvent coordinates.[30−32] Only in the limit of $m \rightarrow \infty$ (or some number of the order of magnitude of the number of atoms in a macroscopic system) can this treatment truly mimic a dissipative solvent. Nevertheless, one can sometimes get a good quantitative approximation to the $m = \infty$ limit with m as small as 5.[10] The adequacy of restricting the number of effective solvent coordinates to be small is problem dependent,[16] but $m = 1$ clearly provides a logical starting point for exploratory studies of nonequilibrium effects.

Not only will we examine improving on the equilibrium solvation result by including nonequilibrium solvation through $G_{\mathrm{NES}}(\mathbf{x}, y)$, but also we will consider approximating the full equilibrium solvation result by the separable equilibrium solvation[2] approximation. Thus our hierarchy of methods has three tiers: (i) separable equilibrium solvation, denoted SES, in which free energies of solvation are added to a gas-phase reaction path (ii) (full) equilibrium solvation, denoted ESP (for equilibrium solvation path) to denote that the reaction path or perhaps just the critical configuration along the reaction path is optimized in the presence of equilibrium solvation forces, and (iii) nonequilibrium solvation, denoted NES. Since we employ a formulation of variational transition state theory with multidimensional tunneling contributions in terms of reaction paths,[4−6] it is useful to point out here that the SES calculation is based on the gas-phase reaction path,[33−36] denoted GRP, which is based on the gas-phase potential energy surface $V(\mathbf{x})$ and passes through the gas-phase saddle point. In contrast the ESP calculation involves a reaction path based on $W(\mathbf{x})$; this reaction path (like the dynamics calculations based on it) is called the equilibrium solvation path[12] (ESP). Finally, the NES calculation involves a reaction path through a $(3N + m)$-dimensional space (in the present paper, we have $m = 1$, but the theory is more general); this reaction path is based on $W(\mathbf{x}, y)$ and is called the nonequilibrium solvation path or NESP. Any of these reaction paths may be defined by the steepest-descents prescription,[33−36] if desired, i.e., one may use the minimum-energy path from reactants-to-products on $V(\mathbf{x})$, $W(\mathbf{x})$, or $w(\mathbf{x}, y)$ (more generally $w(\mathbf{x}, \mathbf{y})$).

Section 2 presents the theoretical formulation of nonequilibrium solvation effects used here. Section 3 give details of an application to reaction R1. Section 4 presents the results and discussion, and Section 5 contains concluding remarks.

2. Theory

There have been numerous attempts to include nonequilibrium solvation effects in the transition state theory of condensed-phase reactions.[9−13,23,37−53] In the present work, we will use the generalized

(19) Tucker, S. C.; Truhlar, D. G. *J. Am. Chem. Soc*. **1990**, *112*, 3347.
(20) Marcus, R. A. *J. Chem. Phys*. **1956**, *24*, 979.
(21) Ovchinnikova, M. Y. *Sov. J. Chem. Phys*. **1986**, *4*, 1.
(22) Basilevsky, M. V.; Chudinov, G. E.; Napolov, D. W. *J. Phys. Chem*. **1993**, *97*, 3270.
(23) Ruiz-López, M. F.; Rinaldi, D.; Bertrán, J. *J. Chem. Phys*. **1995**, *103*, 9249.
(24) Chambers, C. C.; Hawkins, G. D.; Cramer, C. J.; Truhlar D. G. *J. Phys. Chem*. **1996**, *100*, 16385.
(25) (a) Giesen, D. J.; Gu, M. Z.; Cramer, C. J.; Truhlar, D. G. *J. Org. Chem*. **1996**, *61*, 8720. (b) Giesen, D. J.; Chambers, C. C.; Cramer, C. J.; Truhlar, D. G. *J. Phys. Chem*. **1997**, *101*, 2061. (c) Giesen, D. J.; Hawkins, G. D.; Liotard, D. A.; Cramer, C. J.; Truhlar, D. G. *Theor. Chem. Acc*. **1997**, *98*, 85.
(26) Hawkins, G. D.; Cramer, C. J.; Truhlar, D. G. *J. Phys. Chem. B* **1998**, *102*, 3257.
(27) (a) Zhu, T.; Li, J.; Hawkins, G. D.; Cramer, C. J.; Truhlar, D. G. *J. Chem. Phys*. **1998**, *109*, 9117. (b) Li, J.; Hawkins, G. D.; Cramer, C. J.; Truhlar, D. G. *Chem. Phys. Lett*. **1998**, *288*, 293. (c) Li, J.; Zhu, T.; Hawkins, G. D.; Winget, P.; Liotard, D. A.; Cramer, C. J.; Truhlar, D. G. *Theor. Chem. Acc*., in press.
(28) Cramer, C. J.; Truhlar, D. G. In *Solvent Effects and Chemical Reactivity*; Tapia, O., Bertrán, J., Eds.; Kluwer: Dordrecht, The Netherlands, 1980; pp 1−80.
(29) (a) Cramer, C. J.; Truhlar, D. G. *J. Am. Chem. Soc*. **1991**, *113*, 8305. Erratum: **1991**, *113*, 9901. (b) Cramer; C. J.; Truhlar, D. G. *Science* **1992**, *256*, 213. (c) Giesen, D. J.; Cramer, C. J.; Truhlar, D. G. *J. Phys. Chem*. **1995**, *99*, 7137.
(30) Ford, G. W.; Kac, M.; Mazur, P. *J. Math. Phys*. **1973**, *9*, 215.
(31) Zwanzig, R. *J. Stat. Phys*. **1973**, *9*, 215.
(32) Caldeira, A. O.; Leggett, A. J. *Ann. Phys. (N.Y.)* **1983**, *149*, 374.
(33) Marcus, R. A. *Discuss. Faraday Soc*. **1967**, *44*, 7.
(34) Shavitt, I. *J. Chem. Phys*. **1968**, *49*, 4048.
(35) Truhlar, D. G.; Kuppermann, A. *J. Am. Chem. Soc*. **1971**, *93*, 1840.
(36) Fukui, K. *Acc. Chem. Res*. **1981**, *14*, 363.
(37) Kramers, H. A. *Physica* **1940**, *7*, 284.
(38) Takeyama, N. *Experientia* **1971**, *17*, 425.
(39) (a) Grote, R. T.; Hynes, J. T. *J. Chem. Phys*. **1980**, *73*, 2715. (b) van der Zwan, G.; Hynes, J. T. *J. Chem. Phys*. **1982**, *76*, 2993. (c) *Ibid*. **1983**, *78*, 4174. (d) van der Zwan, G.; Hynes, J. T. *Chem. Phys*. **1984**, *90*, 21. (e) Hynes, J. T.; Kim, H. J.; Mathis, J. R.; Timoneda, J. Juanos *J. Mol. Liq*. **1993**, *57*, 53.
(40) (a) Kurz, J. L.; Kurz, L. C. *Isr. J. Chem*. **1985**, *26*, 239. (b) Kurz, J. L. *J. Am. Chem. Soc*. **1989**, *111*, 8631.
(41) (a) Bergsma, J. P.; Gertner, B. J.; Wilson, K. R.; Hynes, J. T. *J. Chem. Phys*. **1987**, *86*, 1356. (b) Gertner, B. J.; Wilson, K. R.; Zichi, D. A.; Lee, S.; Hynes, J. T. *Faraday Discuss. Chem. Soc*. **1988**, *85*, 297. (c) Gertner, B. J.; Wilson, K. R.; Hynes, J. T. *J. Chem. Phys*. **1990**, *90*, 3537.

Langevin approach with the single-oscillator approximation of Garrett and Schenter,[13] and we will show how it can be used in conjunction with a full variational transition state theory calculation including optimized multidimensional tunneling.

2.1. Hamiltonian. To include nonequilibrium solvation effects we add a solvent coordinate y using the approximation of a single harmonic oscillator linearly coupled to the reaction coordinate. In this approximation the Hamiltonian for calculating the free energy of the generalized transition states becomes

$$H = T_{\text{solute}} + W(\mathbf{x}) + \frac{p_y^2}{2\mu} + \frac{1}{2}F(y - \mathbf{C}^{\mathrm{T}}(\mathbf{x} - \mathbf{x}^{\ddagger}))^2 \qquad (5)$$

where $\mathbf{x}$ denotes the solute mass-scaled Cartesian coordinates (in terms of which we may write the reaction coordinate s and the other solute coordinates), $\mathbf{x}^{\ddagger}$denotes the equilibrium solvation saddle point values of the solute coordinates, y is an effective solvent coordinate, p_y is its conjugate momentum, T_{solute} is the solute's kinetic energy, W is the potential of mean force (equal to the gas-phase potential plus the equilibrium free energy of solvation for that $\mathbf{x}$), μ is the scaling mass[4] (which must and will cancel out and have no effect on the results), F is a bath force constant, $\mathbf{C}$ is a solute-bath coupling vector with $3N$ components C_i (where N is the total number of atoms), and T denotes a transpose. Following Garrett and Schenter,[13] the bath parameters F and C_i are determined from an analytic expression for the friction kernel which is in a Gaussian form. Therefore, the force constant is

$$F = \frac{\pi^2\mu}{16\tau^2} \qquad (6)$$

and the elements of the coupling vector are

$$C_i = \left[\frac{16\tau\tilde{k}T}{\pi^2 D_i \mu}\exp\left(\frac{-\pi^2}{32}\right)\right]^{1/2} \qquad (7)$$

where $\tilde{k}$ is Botzmann's constant, T is temperature, τ is the solvation time (which is σ in ref 13), and D_i is the diffusion constant of the atom k_i corresponding to Cartesian coordinate i. Since the reactant free energy is an equilibrium quantity, C_i is set equal to zero at reactants for calculating reactant free energies.

Note that although eqs 5−7 do not explicitly involve electrostatics (e.g., the solute dipole moment and partial atomic charges do not appear), the quantities τ and D_i result from the collective operation of all solute−solvent forces, and hence the "correct" values of these quantities implicitly include electrostatics, hydrogen bonding, electron correlation, and so forth. In fact we will explicitly take account of electrostatics and first-solvent shell effects when we estimate numerical values for C_i and τ as discussed in Section 2.2.

From eq 1, we can write the effective potential as

$$w(\mathbf{x}, y) = W(\mathbf{x}) + \frac{1}{2}F(y - \sum_{i=1}^{3N} C_i\,(x_i - x_i^{\ddagger}))^2 \qquad (8)$$

Note that we can solve for the equilibrium value y_{eq} of y by

$$0 = \frac{\partial}{\partial y}(y - \sum_{i=1}^{3N} C_i\,(x_i - x_i^{\ddagger}))^2|_{y=y_{\text{eq}}} \qquad (9)$$

Therefore,

$$y_{\text{eq}} = \sum_{i=1}^{3N} C_i\,(x_i - x_i^{\ddagger}) \qquad (10)$$

Thus the last term in eq 5 can be written as $^1/_2F(y - y_{\text{eq}})^2$. As stated above, $\mathbf{C}$ is nonzero only for calculating fluxes (e.g., free energies of transition states, which are quasi-equilibrium quantities, not true variables of equilibrium thermodynamics), not for calculating equilibrium properties such as reactant free energies.

From eq 8, we can express the $(3N + 1)$-dimensional gradient as

$$\nabla w = \begin{pmatrix} \dfrac{\partial W}{\partial x_j} - C_j F(y - \sum_{i=1}^{3N} C_i(x_i - x_i^{\ddagger})) \\ \vdots \\ F(y - \sum_{i=1}^{3N} C_i(x_i - x_i^{\ddagger})) \end{pmatrix} \qquad (11)$$

where $j = 1, ..., 3N$. The Hessian matrix can be written as

$$\nabla^2 w = \begin{pmatrix} \dfrac{\partial^2 W}{\partial x_i \partial x_j} + FC_iC_j & \cdots & -FC_i \\ \vdots & \vdots & \vdots \\ -FC_j & \cdots & F \end{pmatrix} \qquad (12)$$

where $i, j = 1, ..., 3N$. Notice that in the limit of zero coupling ($\mathbf{C} = 0$), the Hessian matrix is reduced to a block diagonal form of a $(3N \times 3N)$ matrix and a force constant obtained from the collective solvent coordinate. In this case, the vibrational frequencies of the solute are the same as the ESP approximation plus a "pure" solvent mode of frequency (in radians)

$$\omega = \left(\frac{F}{\mu}\right)^{1/2} = \frac{\pi}{4\tau} \qquad (13)$$

In wavenumbers this is

$$\bar{\nu} = \frac{\omega}{2\pi c} = \frac{1}{8c\tau} \qquad (14)$$

The generalized transition state vibrational partition functions along a reaction path arise from motions in a space orthogonal to overall translation and rotation and to the reaction coordinate.[4] These motions may be separated (to first order) by constructing a Cartesian projection operator[54] that describes the overall translation, rotation, and reaction coordinate direction motion of the solute molecule, and then applying this operator to "filter" these motions from the force constant matrix. Alternatively one may describe the vibrational motion in terms of curvilinear internal coordinates by applying the Wilson ***GF*** matrix method[55,56] to transform the force constant matrix of eq 12 into internal coordinates,[55−58] projecting out the reaction coordinate direction in

(42) (a) Hwang, J.-K.; Warshel, A. *J. Am. Chem. Soc*. **1987**, *109*, 715. (b) Hwang, J.-K.; King, G.; Creighton, S.; Warshel, A. *J. Am. Chem. Soc*. **1988**, *110*, 5297.

(43) Dakhnovskii, Y. I.; Ovchinnikov, A. A.; Semenov, M. B. *Mol. Phys*. **1988**, *63*, 497.

(44) Tucker, S. C. *J. Phys. Chem*. **1993**, *97*, 1596.

(45) Benjamin, I.; Lee., L.; Lloyd, L.; Li, Y. S.; Liu, A.; Wilson, K. R. *Chem. Phys*. **1991**, *152*, 1.

(46) Voth, G. A. *J. Chem. Phys*. **1992**, *97*, 5908.

(47) (a) Bianco, R.; Miertus, S.; Persico, M.; Tomasi, *J. Chem. Phys*. **1992**, *168*, 281. (b) Aguilar, M.; Bianco, R.; Miertus, S.; Persico, M.; Tomasi, *J. Chem. Phys*. **1993**, *174*, 397.

(48) (a) Berezhkovskii, A. M. *Chem. Phys*. **1992**, *164*, 331. (b) Berezhkovskii, A. M.; Zitserman, V. V. *Chem. Phys*. **1992**, *164*, 241. (c) Berezhkovskii, A. M. *J. Chem. Phys*. **1994**, *100*, 5949. (d) Berezhkovskii, A. M.; Dudko, S. A.; Zitserman, V. V. *Chem. Phys*. **1994**, *187*, 275. (e) Berezhkovskii, A. M.; Dudko, S. A. *J. Mol. Liq*. **1994**, *60*, 251.

(49) Nagaoka, Y.; Okuno, Y.; Yoshida, N.; Yamabe, T. *Int. J. Quantum Chem*. **1994**, *51*, 519.

(50) Muller, R. P.; Warshel, A. *J. Phys. Chem*. **1995**, *99*, 17516.

(51) Assfeld, X.; Garapon, J.; Rinaldi, D.; Ruiz-Lopez, M. F.; Rivail, J. L. *J. Mol. Struct. (THEOCHEM)* **1996**, *271*, 107.

(52) McRae, R. P.; Schenter, G. K.; Garrett, B. C. *J. Chem. Soc., Faraday Trans*. **1997**, *93*, 997.

(53) Warshel, A.; Bentzien, J. In *Transition State Modeling for Catalysis*; Truhlar, D. G., Morokuma, K., Eds.; ACS Symposium Series 721; American Chemical Society: Washington, DC, 1999; p 489.

(54) Miller, W. H.; Handy, N. C.; Adams, J. E. *J. Chem. Phys*. **1980**, *72*, 99.

(55) Wilson, E. B., Jr.; Decius, J. C.; Cross, P. C. *Molecular Vibrations*; McGraw-Hill: New York; 1955.

(56) Califano, S. *Vibrational States*; Wiley: New York; 1976.

(57) (a) Jackels, C. F.; Gu, Z.; Truhlar, D. G. *J. Chem. Phys*. **1995**, *102*, 3188. (b) Nguyen, K. A.; Jackels, C. F.; Truhlar, D. G. *J. Chem. Phys*. **1996**, *104*, 6491.

internal coordinates,[57] and then transforming the force constant matrix back to Cartesian coordinates. Both of these methods result in a projected force constant matrix in terms of Cartesian coordinates which may then be used to evaluate the vibrational frequencies. In the present work, we use the latter method to project out the translational, rotational, and reaction coordinate direction. The curvilinear coordinate method is more physical for most cases in the gas phase,[57−59] and for the same reason it should be more physical for most cases in liquid solution.

We can express the potential of mean force $W(\mathbf{x})$ in eq 2 as a Taylor expansion in terms of the displacements of atomic Cartesian coordinates x_i from a reference structure x_i^0

$$W = W_0 + \sum_i^{3N} G_i(x_i - x_i^0) + \frac{1}{2}\sum_{i,j}^{3N} F_{ij}(x_i - x_i^0)(x_j - x_j^0) + ... \quad (15)$$

or in terms of the displacements of curvilinear internal coordinates q_i

$$W = W_0 + \sum_i^{F'} g_i(q_i - q_i^0) + {}^1/_2\sum_{i,j}^{3N} f_{ij}(q_i - q_i^0)(q_j - q_j^0) + ... \quad (16)$$

where F' denotes total number of the internal coordinates ($\geq(3N-5)$ for linear molecules, $\geq(3N-6)$ for polyatomic molecules, with the equality for nonredundant internal coordinates and the inequality for redundant internal coordinates). Also, a curvilinear internal coordinate q_i can be expressed as a power series in Cartesian displacement coordinates x_i

$$q_i = \sum_j^{3N} B_{ij}(x_j - x_j^0) + {}^1/_2\sum_{j,k}^{3N} C^i_{jk}(x_j - x_j^0)(x_k - x_k^0) + ... \quad (17)$$

in which B_{ij} is an element of the Wilson **B** matrix

$$B_{ij} = \left(\frac{\partial q_i}{\partial x_j}\right)\Bigg|_{\{x_j\}=\{x_j^0\}}, \qquad i = 1, ..., F; j = 1, ..., 3N \quad (18)$$

and C^i_{jk} is an element of the tensor $\mathbf{C}^i$

$$C^i_{jk} = \left(\frac{\partial q_i}{\partial x_j \partial x_k}\right)\Bigg|_{\{x_j\}=\{x_j^0\}}, \qquad i = 1, ..., F; j, k = 1, ..., 3N \quad (19)$$

(The $\mathbf{C}^i$ tensor should not be confused with the coupling vector of eq 7.) The algorithms for evaluating the generalized normal mode vibrational frequencies using Wilson ***GF*** matrix method are described in detail in previous papers.[57,58] In present work, using method (ii), we take $q_{F+1} = y$, and we only need to extend the dimensions of the **B** matrix and $\mathbf{C}^i$ tensor by 1 for the extra degree of freedom (the solvent coordinate y) and give a value to the $(3N+1, 3N+1)$ element of the diagonal reciprocal mass tensor[55] μ. We assign values to the elements of **B** and $\mathbf{C}^i$ by assuming that the collective solvent coordinate remains "pure" when we transform from the redundant or nonredundant internal coordinate system to Cartesian coordinates. This corresponds to taking the $(F+1, 3N+1)$ element of the **B** matrix, which indicates the $(\partial y/\partial y)$ derivative, equal to 1; and the other elements in the last row and column of **B** and of the values of the elements in the extended parts of the $\mathbf{C}^i$ tensors are set equal to zero. As a result, a "solvent mode" with a large contribution from y in the eigenvector is observed after diagonalizing the projected Hessian matrix. We set $\mu_{3N+1,3N+1}$ equal to the scaling mass μ introduced in eq 5. (When this is done the resulting rate constants are independent of μ, as they should be.) There is considerable flexibility in defining internal coordinates, and these choices seem intuitive.

To carry out dynamics calculations, we have to add a pure solvent contribution to the zero-point energy (ZPE) and vibrational partition functions of the reactant and product. Unlike the saddle point and generalized transition states, the solvent mode is not coupled to the other modes at the reactants and products, but instead has the uncoupled frequency[52] of eq 13 or 14. This frequency is also used in interpolation schemes (such as dual-level[60] and mapped IVTST[61] calculations).

The solute−solvent coupling potential in eq 5 is an approximation to a more general expression.[10,30,31,52] This model is very general, but other more specific models may allow more physical low-order modeling in individual cases. For example, Hynes and co-workers have considered a variety of models for generalized Langevin equations, attempting to capture the physics of solvent motion more completely for specific cases.[39] In ref 11, a general set of effective solvent coordinates was defined, and expressions for the effective force constant in terms of the generalized Born model of the electrostatic component of solvation were derived. The present model is general enough to treat cases where the dominant coupling mechanism is electrostatic (e.g., dipolar), but it is more general and is also applicable for other mechanisms of solute−solvent coupling. There could be advantages in focusing on electrostatic mechanisms in some cases, when the more general formalism may be appropriate in others. Hwang et al.[42] have presented a model that includes nonequilibrium solvation without involving a separate calculation of equilibrium solvation. This was done by searching for the transition state in a combined solute−solvent space which accounts explicitly for solvent-induced dipoles.

2.2. Solvent Parameters. The present model for nonequilibrium solvation effects involves two kinds of parameters, a coupling strength and a solvation time.

2.2.1. Coupling Strength and Dynamical Participation Factors. The coupling strength is determined from eq 7, in which D_i is treated as an effective diffusion constant for atom k (where i is one of the Cartesian coordinates of atom k). The effective diffusion constant is determined from a prototype diffusion constant that gauges the intrinsic strength of solute−solvent coupling for a given type of solute fragment in a given solvent and from a dynamical participation factor that gauges the actual exposure of the given atom of the solute to solvent at a particular solute geometry. A small, effective diffusion constant of atom or fragment X in solvent S corresponds to strong X−S coupling, but if X is only partially exposed to solvent at the transition state (due to being buried by the rest of the molecular structure), then the X−S coupling in that situation is smaller. The dynamical participation factors may be calculated from solvent-accessible surface areas,[62] from electric polarization fractions,[63] or from atomic contributions to free energies of solvation. Using solvent-accessible surface area emphasizes the shortest-range interactions, and using electric polarization fractions emphasizes the longer-range ones, whereas using free energies of solvation weights both types of contributions. We will present results based on both surface areas and free energies to test the sensitivity to such choices.

The coupling strength for atom k is determined from a prototype diffusion constant multiplied by a participation fraction f_k. We define the effective diffusion constant D_k for atom k in the solute by

$$D_k = f_k^{-1} D_k^{(\text{proto})} \quad (20)$$

where $D_k^{(\text{proto})}$ is the diffusion constant of a prototype model, for example, $D_k^{(\text{proto})}$ of a hydrogen atom is taken the atomic hydrogen diffusion constant, $D_k^{(\text{proto})}$ of a carbon atom in an alkyl group may be taken as the diffusion constant of methane, and $D_k^{(\text{proto})}$ of a hydroxylic oxygen atom is taken as the diffusion constant of water. We consider two schemes for estimating f_k.

In scheme A we use the solvent-accessible surface area[62] A_k of atom k. Thus

(58) (a) Chuang, Y.-Y.; Truhlar D. G. *J. Chem. Phys.* **1997**, *107*, 83. (b) Chuang, Y.-Y.; Truhlar, D. G. *J. Phys. Chem.* A. **1998**, *102*, 242.

(59) Natanson, G. A.; Garrett, B. C.; Truong, T. N.; Joseph, T.; Truhlar, D. G. *J. Chem. Phys.* **1991**, *94*, 7875.

(60) (a) Hu, W.-P.; Liu, Y.-P.; Truhlar, D. G. *J. Chem. Soc., Faraday Trans.* **1994**, *90*, 1715. (b) Chuang, Y.-Y., Truhlar, D. G. *J. Phys. Chem. A* **1997**, *101*, 3808; **1997**, *101*, 8741(E). (c) Chuang, Y.-Y.; Corchado, J. C.; Truhlar, D. G. *J. Chem. Phys.* **1999**, *110*, 550.

(61) Corchado, J. C.; Coitiño, E. L.; Chuang, Y.-Y.; Fast, P. L.; Truhlar, D. G. *J. Phys. Chem.* **1998**, *102*, 2424.

(62) Lee, B.; Richards, F. M. *J. Mol. Biol.* **1971**, *55*, 379.

(63) Cramer, C. J.; Truhlar, D. G. *Chem. Phys. Lett.* **1992**, *198*, 74; **1993**, *202*, 567(E).

$$f_k = \min\begin{Bmatrix} A_k/A_k^{(\mathrm{proto})} \\ 1 \end{Bmatrix} \tag{21}$$

where A_k is the solvent-accessible surface area of atom k in the solute under consideration at the solute geometry under consideration, and $A_k^{(\mathrm{proto})}$ is the solvent accessible surface area of atom k in the prototype. Scheme A seems very reasonable on the basis of dimensional analysis, but it may be questionable when dynamic aspects of solvation are dominated by long-range forces.

Scheme G takes advantage of the fact that SM*x* models allow an atom-by-atom decomposition of the free energy of solvation. Thus the standard state (0) free energy of solvation of a system at a fixed-geometry **x** is[26,27]

$$\Delta G_S^0(\mathbf{x}) = \Delta G_{EP}(\mathbf{x}) + G_{CDS}(\mathbf{x}) \tag{22}$$

and its two parts are each decomposed on an atom-by-atom basis:[63]

$$\Delta G_{EP}(\mathbf{x}) = \sum_k \Delta G_{EP}(k, \mathbf{x}) \tag{23}$$

and

$$G_{CDS}(\mathbf{x}) = \sum_k G_{CDS}(k, \mathbf{x}) \tag{24}$$

In scheme G we write

$$f_k = \min\left\{ \left| \frac{\Delta G_{EP}(k, \mathbf{x}) + G_{CDS}(k, \mathbf{x})}{\Delta G_{EP}^{(\mathrm{atom})}(k, \mathbf{x}) + G_{CDS}^{(\mathrm{atom})}(k, \mathbf{x})} \right| \right\} \tag{25}$$

where, as explained in the following paragraphs, $\Delta G_{EP}^{(\mathrm{atom})}(k)$ is the EP solvation free energy for an isolated atom k calculated using the Born equation[64] with intrinsic Coulombic radius ρ_k and using the partial charges $q_k(x)$ obtained from the same geometry **x**, and $\Delta G_{CDS}^{(\mathrm{atom})}(k,\mathbf{x})$ is the CDS component of the solvation free energy for an isolated atom k calculated with the atomic surface tension σ_k that atom k has in the molecule of interest at geometry **x**. If the functional group in the prototype differs sufficiently from that in the molecule under consideration, one might replace q_k in the atomic Born calculation by q_k from the prototype, but that is not done here.

In the SM5.42 model[27] used here

$$G_{CDS}(k, \mathbf{x}) = \sum_k \sigma_k(\mathbf{x}) A_k(\mathbf{x}) \tag{26}$$

and

$$\sigma_k = \sigma_k^{\mathrm{A}}(\mathbf{x}) + \sigma^{\mathrm{M}}(\mathbf{x}) \tag{27}$$

where $\sigma_k^{\mathrm{A}}(\mathbf{x})$ and $\sigma^{\mathrm{M}}(\mathbf{x})$ are the atomic-number-dependent and atomic-number-independent contributions to the geometry-dependent surface tension of atom k, and the $A_k(\mathbf{x})$ is the exposed van der Waals surface area of atom k. Therefore

$$G_{CDS}(k) = \sigma_k(\mathbf{x}) A_k(\mathbf{x}) \tag{28}$$

and

$$G_{CDS}^{(\mathrm{atom})}(k) = \sigma_k(\mathbf{x}) A_k(\mathrm{atom}) \tag{29}$$

The decomposition of ΔG_{EP} is carried out by a method that we have previously[61] called method I. In this method

$$\Delta G_{EP}(k, \mathbf{x}) = \Delta G_{EP}(\mathbf{x}) \frac{G_P(k, \mathbf{x})}{G_P(\mathbf{x})} \tag{30}$$

and

$$\Delta G_{EP}(\mathbf{x}) = \Delta E_E(\mathbf{x}) + G_P(\mathbf{x}) \tag{31}$$

where $\Delta E_E(\mathbf{x})$ is the change in the internal electronic kinetic and Coulombic energy of the whole solute upon equilibrium solvation by the solvent, $G_P(\mathbf{x})$ is the whole electric polarization free energy, and $G_P(k, \mathbf{x})$ is the part of G_P that is attributable to atom k. The latter is easily identified[63] in the SM5.42 solvation model[27] used here because G_P in that model is given by the generalized Born[65−67] equation. Finally

$$\Delta G_{EP}^{(\mathrm{atom})}(k, \mathbf{x}) = -\frac{1}{2}\left(1 - \frac{1}{\epsilon}\right)\frac{q_k^2(\mathbf{x})}{\rho_k} \tag{32}$$

In principle the dynamical partition factors f_k are function of the geometry **x**, but we make the further approximation of evaluating them at the saddle point of the free energy surface $W(\mathbf{x})$ and treating them as constants.

2.2.2. Solvent Response Spectral Profile. The solvation time is taken as having the same values for all atoms of the solute and depends only on the solvent. In the present work, following earlier numerical tests by McRae et al.,[68] we have chosen to use a single time constant, i.e., we characterize the solvent response spectrum by a single frequency. For more accuracy one could use a larger number of effective solvent coordinates, each with its own frequency. However, at the present stage of development this does not seem warranted because the assumption of a single time constant probably leads to smaller error than the many other uncertainties of the theory, such as the estimation of the solute−solvent coupling strength. For example, Tucker[44] found that nonequilibrium effects on reaction rates are determined mainly by two solvent parameters, a single time scale characterizing the solvent response spectral profile and the overall strength of the coupling. Tucker's treatment was based on a one-coordinate treatment of the solute. We use a full atomic representation of the solute, and so we replace the latter by an effective coupling strength for each atom of the solute. However, we retain only a single time constant for all solvent−solute couplings. This seems reasonable in light of the analysis of Maroncelli et al.,[69] which showed that, in many cases, the solvation time constant is primarily a function of solvent properties, not solute properties. The analysis of Maroncelli et al. is based on fast underdamped solvent motion in the inertial streaming regime. This kind of motion is known to account for more than 50% of solvent relaxation in most cases.[69−71] On the basis of this model, Maroncelli et al. gave a simple approximation to the solvation relaxation time τ which can be easily estimated from the dipole moment, moments of inertia, density, dielectric constant, and temperature of any polar solvent. This model leads to $\tau = 10$ fs for water, in good agreement with the value of 8.5 fs estimated by Garrett and Schenter[13] from the molecular dynamics simulations of Palmer and Schenter.[72] We recommend using the formula of Maroncelli et al.[69] as a standard that can be widely tested against experiment, and we shall use $\tau = 10$ fs in the present work. It is interesting to note that this is much faster than values calculated by assuming overdamped solvent relaxing by a diffusive mechanism; in that case the solvation response time should be equal to the longitudinal relaxation time τ_L, which itself may be estimated from the Debye time (or transverse relaxation time) τ_D, the dielectric constant ϵ, and the refractive index n. One obtains[73,74]

(64) Born, M. *Z. Phys.* **1920**, *1*, 45.
(65) Hoijtink, G. J.; de Boer, E.; VanderMeij, P. H.; Weiland, W. P. *Recl. Trav. Chim. Pays-Bas* **1956**, *75*, 487.
(66) Peradejordi, F. *Cah. Phys.* **1963**, *17*, 343.
(67) Jano, I. *Compt. Read. Acad. Sci. Paris* **1965**, *261*, 103.
(68) McRae, R. P.; Schenter, G. K.; Garrett, B. C.; Haynes, G. R.; Voth, G. A.; Schatz, G. C. *J. Chem. Phys.* **1992**, *97*, 7392.
(69) Maroncelli, M.; Kumar, V. P.; Papazyan, A. *J. Phys. Chem.* **1993**, *97*, 13.
(70) Bruell, M.; Hynes, J. T. *J. Phys. Chem.* **1992**, *96*, 4068.
(71) Hynes, J. T. In *Ultrafast Dynamics of Chemical Systems*; Simon, J. D., Ed.; Kluwer: Dordrecht; 1994; p 345.
(72) Palmer, B. J.; Garrett, B. C. *J. Chem. Phys.* **1993**, *98*, 4047.
(73) Zusman, L. D. *Soviet Phys. JETP* **1976**, *42*, 794.

$$\tau_L = \frac{n^2}{\epsilon}\tau_D \quad (33)$$

which yields $\tau_L = 200$ fs for water. Molecular dynamics simulations[69−71] favor the faster values obtained from the Maroncelli et al. formula, not the slower τ_L value. However, Hwang et al.[42] advocated obtaining the solvation time from the autocorrelation of a diabatic energy gap rather than the velocity autocorrelation function, and this leads to slower values. Although the shorter (faster) times are more consistent with experiment,[68] as a sensitivity check we will also report calculations based on longer (slower) solvation times. Making the solvent slower need not increase the NES effects since slower solvents may couple less strongly to the reactive modes in some cases.

For $\tau = 10$ fs, eq 14 gives a frequency of 417 cm^{-1}, and for $\tau = 200$ fs, it gives 21 cm^{-1}. For comparison we note that $\tau = 8.5$ fs yields $\bar{\nu} = 491$ cm^{-1}.

2.3. Software. The dynamics calculations all employed direct dynamics techniques,[75] i.e., the energies, solvation free energies, gradients, and Hessians were obtained as needed by electronic structure calculations without the intermediate step of fitting a potential energy surface or potential of mean force surface. The electronic structure calculations employed the HF||AM1-SRP method and were carried out with the GAMESOLRATE program,[76] which is an interface of the POLYRATE dynamics code[77,78] and the GAMESOL electronic structure code.[79] The rate calculations were carried with a modified version 8.2 of POLYRATE-version 8.1,[77] and the methods will eventually be available in later version of POLYRATE. Dynamical participation factors were calculated using AMSOL[80] for Scheme A and GAMESOL[79] for scheme G.

3. Application to R1

Previously, we calculated the aqueous-solution rate constant for the hydrogen atom abstraction from methanol molecule, reaction R1, with two approximations, namely, the separable equilibrium solvation (SES) and the equilibrium solvation path (ESP) approximations.[3] A linear mixing of Hartree−Fock and AM1 with specific reaction parameters (HF||AM1-SRP) was used to calculate the electronic energies, gradients, Hessians, free energies, free-energy gradients, and free-energy Hessians along the reaction path. The parameters of the HF||AM1-SRP method are given in ref 3. After the gas-phase reaction rate constants have been determined, CM2 and SM5.42R parameters are needed for estimating partial charges, dipole moments, and solvation energies; these parameters are discussed in ref 3. The gas- and solution-phase reaction energetics are given in Table 1 for both the SES and ESP approximations.

Table 1. Reaction Energetic and Structural Information[a] for R1

theory	$V^{\ddagger}$ or $W^{\ddagger}$[b]	ΔE or ΔW[c]	$R^{\ddagger}_{H-H}$	$R^{\ddagger}_{H-C}$
best estimate (*g*)[d]	8−10[e]	−5.1		
HF||AM1-SRP (*g*)[d]	7.8	−5.0	0.867	1.277
HF||AM1-SRP (SES)[f]	7.5	−3.0	0.841	1.297
HF||AM1-SRP (ESP)[g]	7.5	−3.6	0.854	1.281

[a] Energies in kcal/mol, bond lengths in Å. The bond distances are those for the making and breaking bonds. [b] Barrier height relative to reactants ($V^{\ddagger}$ for gas phase, $W^{\ddagger}$ in liquid). [c] Energy of reaction, excluding zero-point contributions, relative to reactants (ΔE, which equals ΔV, for gas phase; ΔW in liquid). [d] Gas-phase results. [e] Reference 3. [f] Liquid-phase results with SES approximation. [g] Liquid-phase results with ESP approximation.

Table 2. Atomic Diffusion Coefficients According to Scheme A[a]

atom[b]	A_k	$A_k^{(proto)}$	f_k	$D_k^{(proto)}$	D_k
H	12.34	18.10	0.682	8.0	11.7
X	3.80	18.10	0.210	8.0	38.1
C	11.77	15.40	0.764	1.5	2.0
O	13.98	17.86	0.783	2.3	2.9
Y	8.13	18.10	0.449	8.0	17.8
Z	8.12	18.10	0.449	8.0	17.8
W	8.98	18.10	0.496	8.0	16.1

[a] Areas in $Å^2$, diffusion coefficients in 10^{-5} cm^2 s^{-1}. [b] The labeling of atoms corresponding to the reaction CXYZOW + H → HX + CYZOW.

In the present work, we estimate the nonequilibrium solvation effects for reaction R1. As we discussed in the previous section, the coupling constant C_i is determined by the solvation time (τ) and the effective atomic diffusion constants (D_k). In the present work, we use the value $\tau = 10$ fs which obtained by Maroncelli et al. for most of our calculations; the dynamics calculations are also carried with longer solvation times for comparison.

We then need to estimate the atomic diffusion constants. The first step, as explained in Section 2.2.1, is to specify the prototype model. We use methane ($D^{(proto)} = 1.5 \times 10^{-5}$ cm^2 s^{-1} in water)[81] as a prototype for the C atom, water ($D^{(proto)} = 2.3 \times 10^{-5}$ cm^2 s^{-1} in water)[82] as a prototype for the O atom, and $D^{(proto)} = 8 \times 10^{-5}$ cm^2 s^{-1} for the H atom.[83] Dynamical participation factors were calculated by the two schemes (A and G) described in Section 2.2.1.

For scheme A, we then calculate the surface-accessible-area of the hydrogen atom, saddle point, methanol, methane, and water molecules at the SM5.42/HF||AM1-SRP level. The surface-accessible-area and the calculated atomic diffusion constants are given in Table 2. For scheme G, we obtain the free energy of solvation of the prototype molecules/atom and the saddle point at SM5.42/AM1-SRP level. The atomic diffusion constants evaluated with scheme G are given in Table 3. We then carry out the dynamics calculations using a prerelease version of GAMESOLRATE-version8.1 with the same dynamics parameters from the equilibrium solvation study carried previously.

Although the parameter C_i is called the "coupling constant", eq 8 shows that the coupling between the solvent coordinate *y*

(74) (a) Doubleday: C.; McIver, J. W. Jr.; Page, M. *J. Phys. Chem.* **1988**, *92*, 4367. (b) Baldridge, K. K.; Gordon, M. S.; Steckler, R.; Truhlar, D. G. *J. Phys. Chem.* **1989**, *93*, 5107. (c) Garrett, B. C.; Koszykowski, M. L.; Melius, C. F.; Page, M. *J. Phys. Chem.* **1990**, *94*, 7096. (d) For a review see Truhlar, D. G. Understanding Chemical Reactivity 16. In *The Reaction Path in Chemistry*; Heidrich, D., Ed.; Kluwer: Dordrecht, The Netherlands, 1995; p 229.

(75) McConnell, J. *Rotational Brownian Motion and Dielectric Theory*; Academic: New York, 1980.

(76) Chuang, Y.-Y.; Corchado, J.; Truhlar, D. G. GAMESOLRATE-version 8.1, University of Minnesota, Minneapolis, 1999, based on POLYRATE-version 8.1 and GAMESOL-version 2.2. [http://comp.chem.umn.edu/~gamesolrate]

(77) Steckler, R.; Hu, W.-P.; Liu, Y.-P.; Lynch, G. C.; Garrett, B. C.; Isaacson, A. D.; Melissas, V. S.; Lu, D.-h.; Truong, T. N.; Rai, S. N.; Hancock, G. C.; Lauderdale, J. G.; Joseph, T.; Truhlar, D. G. *Comput. Phys. Commun.* **1995**, *88*, 341.

(78) Chuang, Y.-Y.; Corchado, J. C.; Fast, P. L.; Villà, J.; Coitiño, E. L.; Hu, W.-P.; Liu, Y.-P.; Lynch, G. C.; Nguyen, K.; Jackels, C. F.; Gu, M. Z.; Rossi, I.; Clayton, S.; Melissas, V.; Steckler, R.; Garrett, B. C.; Isaacson, A. D.; Truhlar, D. G. POLYRATE-version 8.1, University of Minnesota, Minneapolis, 1999 [http://comp.chem.umn.edu/polyrate].

(79) Li, J.; Zhu, T.; Hawkins, G. D.; Chuang, Y.-Y.; Liotard, D. A.; Rinaldi, D.; Cramer C. J.; Truhlar, D. G. GAMESOL-version 2.2, University of Minnesota, 1999, based on the General Atomic and Molecular Electronic Structure System (GAMESS) as described in Schmidt, M. W.; Baldridge, K. K.; Boatz, J. A.; Elbert, S. T.; Gordon, M. S.; Jensen, J. H.; Koseki, S.; Matsunaga, N.; Nguyen, K. A.; Su, S. J.; Windus, T. L.; Dupuis, M.; Montgomery, J. A. *J. Comput. Chem.* **1993**, *14*, 1347 [http://comp.chem.umn.edu/gamesol].

(80) Hawkins, G. D.; Giesen, D. J.; Lynch, G. C.; Chambers, C. C.; Rossi, I.; Storer, J. W.; Li, J.; Zhu, T.; Rinaldi, D.; Liotard, D. A.; Cramer, C. J.; Truhlar, D. G. AMSOL-version6.5.3, University of Minnesota, Minneapolis, 1998 [http://comp.chem.umn.edu/~amsol].

(81) *Handbook of Chemistry and Physics*; Lide, D. R., Ed.; CRC: Boca Raton, FL,1994; p 6−253.

(82) Weingartner, H. *Z. Phys. Chem. (Munich)* **1982**, *123*, 129.

(83) Bartels, D., private communication quoted in Garrett and Schenter.[13]

Table 3. Atomic Diffusion Coefficients According to Scheme G[a]

atom[b]	$\Delta G_S^0(k)$	$\Delta G_S^{0,(atom)}(k)$	f_k	$D_k^{(proto)}$	D_k
H	1.20	1.21	0.990	8.0	8.1
X	−0.24	−0.38	0.634	8.0	12.6
C	1.40	1.61	0.870	1.5	1.7
O	−3.22	−4.25	0.757	2.3	3.0
Y	−0.33	1.37	0.242	8.0	33.1
Z	−0.03	0.65	0.042	8.0	192.3
W	−3.53	−22.30	0.158	8.0	50.5

[a] Free energy of solvation in kcal/mol, diffusion coefficients in 10^{-5} cm^2 s^{-1}. [b] The labeling of atoms corresponding to the reaction CX-YZOW + H → HX + CYZOW.

and solute coordinate x_i is actually proportional to the product FC_i; this product is called A_i. For example, using eq 13, eqs 8, 11, and 12 can be written as

$$w(\mathbf{x}, y) = W(\mathbf{x}) + \frac{1}{2}\mu\omega^2 y^2 - \sum_{i=1}^{3N} A_i(x_i - x_i^{\ddagger})y + \frac{1}{2\mu\omega^2}\left[\sum_{i=1}^{3N} A_i(x_i - x_i^{\ddagger})\right]^2 \quad (34)$$

$$\nabla w = \begin{pmatrix} \dfrac{\partial W}{\partial x_j} - A_j + \dfrac{A_j}{\mu\omega^2}\displaystyle\sum_{i=1}^{3N} A_i(x_i - x_i^{\ddagger}) \\ \vdots \\ \mu\omega^2 y - \displaystyle\sum_{i=1}^{3N} A_i(x_i - x_i^{\ddagger}) \end{pmatrix} \quad (35)$$

$$\nabla^2 w = \begin{pmatrix} \dfrac{\partial^2 W}{\partial x_i \partial x_j} + \dfrac{A_i A_j}{\mu\omega^2} & \cdots & -A_i \\ \vdots & & \vdots \\ -A_j & \cdots & \mu\omega^2 \end{pmatrix} \quad (36)$$

where $j = 1, ..., 3N$. Here, ω is the frequency of the pure solvent mode, which according to eq 13, is inversely proportional to the solvation time, and A_j determines the coupling between solute coordinate x_i and solvent coordinate y. Thus, we will perform some calculations in which τ is varied at fixed values of A_i.

The above considerations fix the parameters in the Hamiltonian. After that, the dynamics calculations proceed just as in the equilibrium solvation path case except that there are $3N + 1$ coordinates instead of $3N$. We consider four levels of dynamical theory:

CVT[4,5,15]	canonical variational transition state theorywithout tunneling
CVT/ZCT[4,5,15] CVT	with zero-curvature tunneling
CVT/SCT[82,83] CVT	with small-curvature tunneling
CVT/μOMT[84] CVT	with microcanonical optimized multidimensional tunneling

These methods are all explained in detailed elsewhere,[4,5,15,84−86] and therefore we limit ourselves to a one-sentence recap of each method. The CVT approximation is based on finding the dynamical bottleneck that has the maximum free energy of activation; vibrations are quantized, but motion along the reaction coordinate is classical. The CVT/ZCT approximation includes tunneling along the minimum energy path (MEP). The CVT/SCT approximation allows the tunneling paths to "cut the corner",[87−89] but it confines the path within a hypercylindrical tube centered on the MEP; the width of the tube in the direction of any vibration is the distance between the zero-point level classical turning points of that vibration, and the direction of corner cutting is determined by the internal centrifugal force due to curvature of the MEP. The CVT/μOMT approximation allows the corner cutting path to leave the MEP tube and, if more favorable, to correspond to a straight-line path[90−92] (shortest possible path) in isoinertial coordinates. These methods have all been validated against accurate quantum mechanical calculations for few-body systems where accurate quantal calculations are possible.[93]

Anticipating the results, we note that for the present reaction, the μOMT result is almost the same as the large-curvature limit,[86,90−92] in which the tunneling *is* most dominated by the straight-line path since the reaction path curves back on itself so strongly in isoinertial coordinates.

4. Results and Discussion

Our "best" calculation is the one with our highest dynamical level, CVT/μOMT, and with our best estimates of the parameters, i.e., $\tau = 10$ fs and scheme G for D_k. This calculation yields a 52% decrease in the reaction rate as compared to the equilibrium solvation path (ESP) calculations. Since the ESP calculations predicted a factor of 1.99 speedup as compared to the gas-phase, the resulting prediction for the ratio of the rate constant in the liquid phase to the rate constant in the gas phase is $1.99 \times (1 - 0.52) = 0.96$, i.e., a 4% slowing down. This still agrees with experiment within experimental error, since the experimental result has been estimated to be a factor of 1.8 ± (factor of 3), i.e., between 0.6 and 5.4, by us,[3] and a factor of 1.23 (without an error bar) by Mezyk and Bartels.[94] (The uncertainty in the experimental result is primarily due to the uncertainty in the absolute value in the gas phase.) Next we present results for several other choices of the parameters because they increase understanding.

Figure 1 shows the effective potential along the nonequilibrium reaction path at 298 K. The effective potential V_{eff} is the sum of the potential of mean force ($W(\mathbf{x}, y)$ in eq 3) and the ZPE, i.e., it is the sum of the Born−Oppenheimer energy, the standard-state free energy of solvation, and the ZPE. The effective potential is shown for three different values of the solvation time τ. In this figure, we observe that the effective barrier height for 10 fs is higher than that for 200 fs, which is closer to the ESP limit, which is 5.59 kcal/mol at the ESP saddle

(84) Lu, D.-h.; Troung, T. N.; Melissas, V. S.; Lynch, G. C.; Liu, Y.-P.; Garrett, B. C.; Steckler, R.; Isaacson, A. D.; Rai, S. N.; Hancock, G. C.; Lauderdale, J. G.; Joseph, T.; Truhlar, D. G. *Comput. Phys. Commun.* **1992**, *71*, 235.

(85) Liu, Y.-P.; Lynch, G. C.; Truong, T. N.; Lu, D.-h.; Truhlar, D. G.; Garrett, B. C. *J. Am. Chem. Soc.* **1993**, *115*, 2408.

(86) Liu, Y.-P.; Lu, D.-h.; Gonzalez-Lafont, A.; Truhlar, D. G.; Garrett, B. C. *J. Am. Chem. Soc.* **1993**, *115*, 7806.

(87) Kuppermann, A.; Adams, J. T.; Truhlar, D. G. In *Electronic and Atomic Collisions*; Cobič, B. C., Kurepa, M. V., Eds.; Institute of Physics: Belgrade, 1973; p 149.

(88) Marcus, R. A.; Coltrin, M. E. *J. Chem. Phys.* **1977**, *67*, 2609.

(89) Skodje, R. T.; Truhlar, D. G.; Garrett, B. C. *J. Chem. Phys.* **1982**, *77*, 5955.

(90) Garrett, B. C.; Truhlar, D. G.; Wagner, A. F.; Dunning, T. H., Jr. *J. Chem. Phys.* **1983**, *78*, 4400.

(91) Bondi, D. K.; Connor, J. N. L.; Garrett, B. C.; Truhlar, D. G. *J. Chem. Phys.* **1983**, *78*, 5981.

(92) Truhlar, D. G.; Gordon, M. S. *Science* **1990**, *249*, 491.

(93) Allison, T. C.; Truhlar, D. G. In *Modern Methods for Multidimensional Dynamic Computations in Chemistry*; Thompson, D. L., Ed.; World Scientific: Singapore, 1998; p 618.

(94) Mezyk, S. P.; Bartels, D. M. *J. Phys. Chem.* **1994**, *98*, 10578.

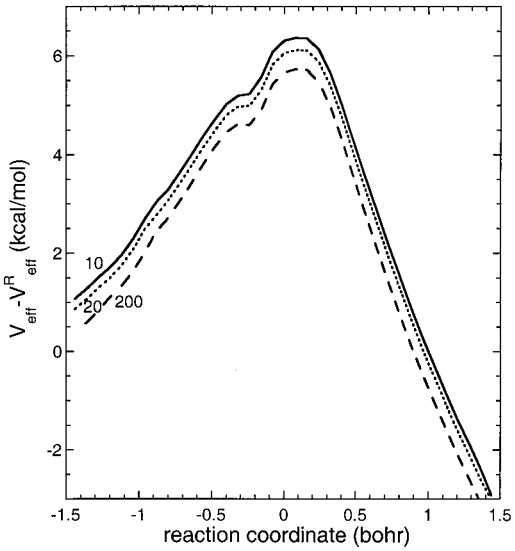

Figure 1. Effective potential along the nonequilibrium reaction path of R1 minus effective effective potential at reactants for three values of the solvation time. The solid curve is for $\tau = 10$ fs, the dotted curve is for $\tau = 20$ fs, and the dashed curve is for $\tau = 200$ fs. All calculations are carried out with the diffusion coefficients evaluated using scheme G. Thus, in the figure, the coupling strength varies with changes in τ according to eq 7.

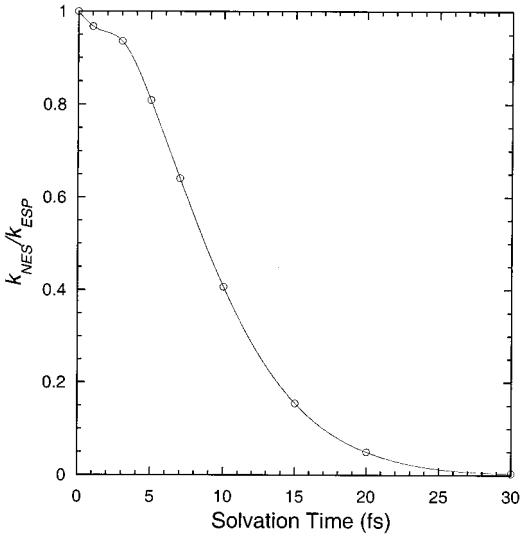

Figure 2. Ratio k_{NES}/k_{ESP} as evaluated by conventional transition state theory. The curve is a polynomial fit. These calculations were performed with constant A_i which is evaluated using $\tau = 10$ fs and the diffusion constants obtained from scheme G.

point and 5.75 kcal/mol at the 298 K ESP variational transition state. This might appear counterintuitive (we expect to reach the equilibrium limit for fast solvent, not slow solvent) until one realizes that the coupling strength is varied if one varies τ with fixed D_k, as was done in Figure 1. In particular, eqs 6 and 7 show that the coupling strength FC_i varies as $\tau^{-3/2}$ where τ is varied at fixed D_k, and this explains why the equilibrium limit is achieved for large τ in this kind of plot.

To examine the dependence of the reaction rate constants on the solvation time (τ) for a fixed strength of the solute coupling to the bath, we used the substitutions introduced in the previous section (eqs 34, 35, and 36), and we varied τ at fixed A_i. The fixed A_i are chosen to be the product of the original F value original C_i calculated with $\tau = 10$ fs and with the diffusion coefficients obtained from scheme G. Figure 2 shows the ratio of the rate constants evaluated using the NES approximation to the rate constants evaluated with the ESP approximation. This ratio tends to 1 as τ tends to zero when we keep the coupling A_i constant. This validates the physical nature of the present formulation because it agrees with the physical picture that if the solvation time becomes smaller, the solvent molecules reorganize faster to accommodate the sudden change in the environment, and therefore the reaction rate constant tends to the equilibrium solvation limit. However, if the solvent molecules require more time to reorganize, the nonequilibrium solvation effect becomes more important. For example, Figure 2 shows that for $\tau \geq 25$ fs, the rate constant evaluated using the NES approximation is more than a factor of 30 smaller than the ESP rate constant.

The choice of τ affects not only the reaction coordinate but also the bound motions of the solute molecule. This is illustrated in Figure 3, where, for discussion purposes, we show the frequencies at the liquid-phase saddle point as a function of τ (again τ is varied with fixed A_i); Figure 4 shows the corresponding variation in the ZPE. At the left-side of Figure 3 ($\tau =$ 1 fs), the solute frequencies are basically the same as for $\tau =$ 0 fs, and the solvent frequency is $\sim$4200 cm^{-1}, which is $\sim$800 cm^{-1} larger than the largest solute frequency. This gap prevents significant solute−solvent mode mixing. For $\tau < 1$ fs, the gap will be even larger since eq 13 shows that the pure solvent mode frequency is inversely proportional to τ. This explains why $k_{NES}/k_{ESP} \approx 1$ for $\tau \leq 1$ fs in Figure 2. Then, as τ increases, it passes through the solute frequencies and mixes with them; Figure 3 shows this process. At $\tau = 5$ fs, the solvent frequency has decreased to $\sim$800 cm^{-1}, and for $\tau = 5-10$ fs it mixes strongly with the low-frequency modes of the solute. When $\tau \gtrsim 25$ fs, the frequencies of the bound modes become much larger, which makes the free energy barrier much higher than the one obtained from the ESP approximation and results in a smaller reaction rate constant. Figure 5 gives a different perspective on solvent−solute mode mixing. It shows how the solvent mode gets pushed down in frequency by coupling to the solute for $\tau > 5$ fs; this in turn increases the other frequencies. This figure dramatically illustrates how the solvent mode mixes strongly with the solute modes for $\tau > 5$ fs.

Recall that the solvent bath is coupled to the Cartesian coordinates of the solute molecule in our formalism. A possible improvement is to couple the bath mode to each of the normal modes of the solute molecule differently; however, this might require more parameters to represent the coupling.

Tables 4 and 5 and Figure 6 show how the aqueous-solution rate constants and their ratios to gas-phase ones depend on the effective atomic diffusion coefficients when $\tau = 10$ fs. In the tables, D_k^A denotes the diffusion constants obtained from scheme A for the dynamical participation factors; D_k^G denotes those from scheme G. Furthermore, $D_k^G/2$ means that the atomic diffusion constants are taken as the half of the D_k^G values, and $2D_k^G$ means that the atomic diffusion constants are taken to be twice the D_k^G values.

First, consider the comparison of results obtained with D_k^A to those obtained with D_k^G (rows 3 and 6 of Tables 4 and 5). It is encouraging the results with $D_k = D_k^A$ agree well with those for $D_k = D_k^G$ because this shows that the model is not overly sensitive to the method used to estimate dynamical participation factors.

Next, consider the dependence on scaling D_k. From eq 7 we see that the coupling constant is inversely proportional to the diffusion constants as is the coupling strength A_i; therefore, Tables 4 and 5 are showing the aqueous solution rate constants

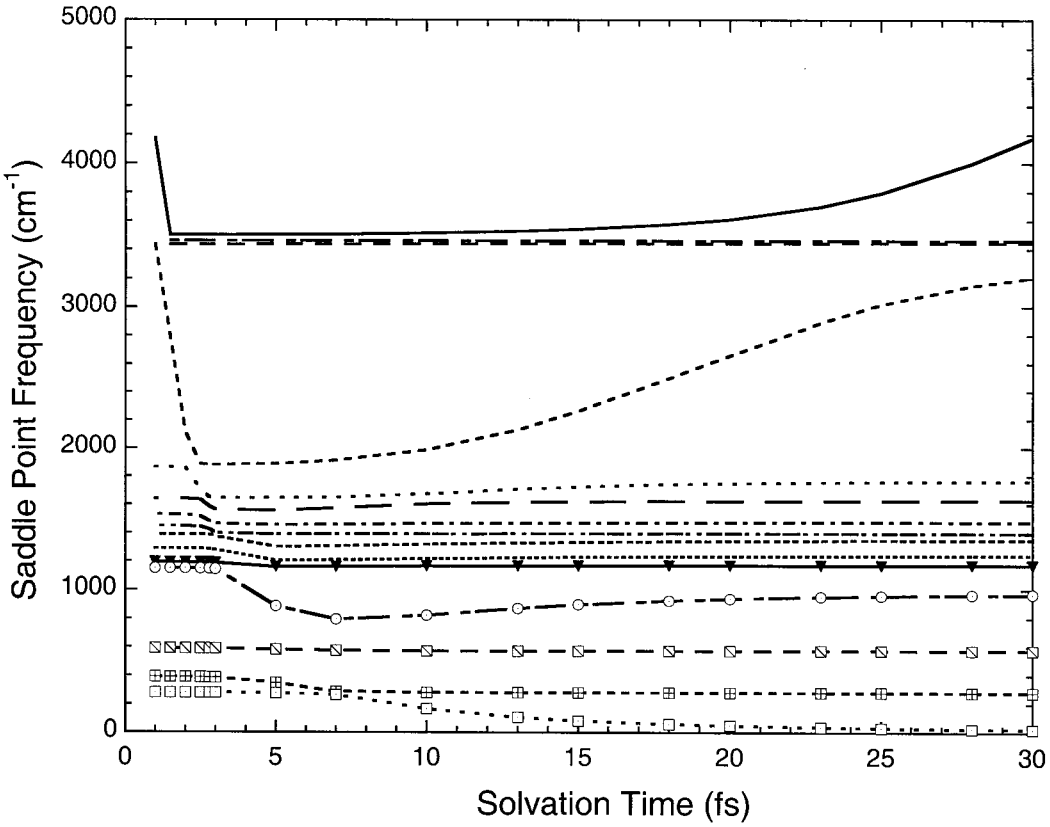

Figure 3. Frequencies of motions transverse to the reaction coordinate for a series of calculations in which τ is varied with A_i fixed as in Figure 2. The frequencies are evaluated at the ESP saddle point location.

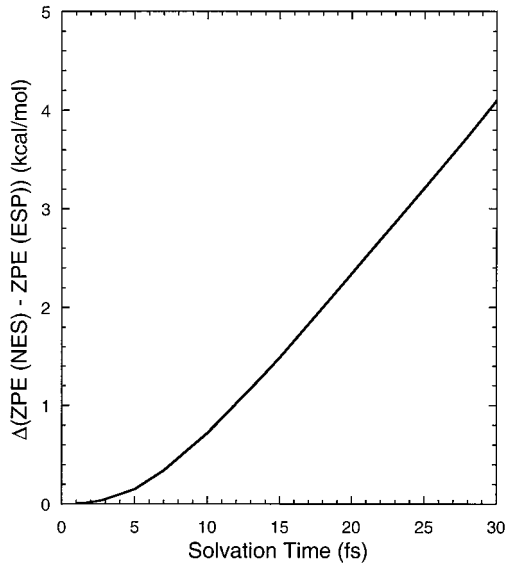

Figure 4. Nonequilibrium solvation effect on the ZPE at the ESP saddle point evaluated with different solvation times τ with A_i fixed as in Figure 2. The solvent modes are included for estimating the ZPEs.

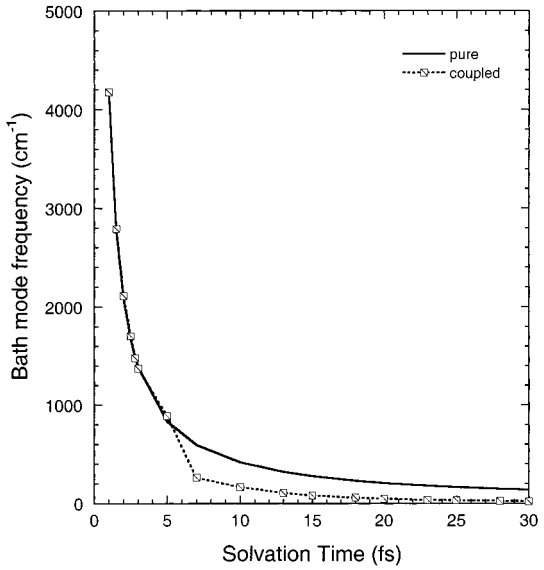

Figure 5. Like Figure 3 except only two modes are shown: the solid curve is the uncoupled bath mode frequency of eq 13, and the dashed curve is the coupled bath mode, i.e., the mode from the NES calculation whose eigenvector has the highest contribution from the bath coordinate.

increase when the coupling strengths decrease at fixed τ. Eventually, they reach the zero-coupling limit, which is the ESP. In the other direction, as the D_k decrease and the coupling strength increases, the calculated rate constants tends to zero. These two trends are precisely as expected, and they confirm again that the theory behaves in a physically realistic fashion.

Typically the inclusion of dynamical coupling to the solvent decreases the tunneling effect as solute−solvent coupling increases. This has been explained by McRae et al.[52] as follows. When solute−solvent coupling is important, the tunneling-path length though all the coordinates is larger than the path length through the solute coordinates alone because the solute "drags" along the bath modes. Thus, the barrier in the mass-scaled coordinate system is effectively widened. The present paper provides the first information about the effect of nonequilibrium solvation on full multidimensional tunneling calculations. Tables 4 and 5 show that the nonequilibrium solvation effect is very similar, independent of whether tunneling is included and whether it is constrained to the small-curvature tube around the MEP. For example, using our best parameters, the nonequilibrium solvation effect is a factor of 0.42 at the CVT dynamical

Table 4. Aqueous Solution Rate Constants[a] of Reaction R1 at 298 K

level	τ^b	D_k	TST[c]	CVT	ZCT[d]	SCT[e]	μOMT[f]
SES			1.7	0.9	2.4	8.7	12.7
ESP	0	∞	2.2	1.9	4.8	16.6	25.9
NES	10	D_k^A	0.79	0.71	1.7	5.6	11.5
NES	10	$D_k^G/4$	0.12	0.12	0.28	0.89	4.1
NES	10	$D_k^G/2$	0.42	0.39	0.95	3.1	7.0
NES	10	D_k^G	0.90	0.81	2.0	6.5	12.4
NES	10	$2D_k^G$	1.4	1.2	3.0	10.1	17.7
NES	10	$4D_k^G$	1.7	1.5	3.8	12.9	21.1
NES	10	$8D_k^G$	2.0	1.7	4.2	14.5	23.1
NES	10	$16D_k^G$	2.1	1.8	4.5	15.4	24.1
NES	10	$20D_k^G$	2.1	1.8	4.6	15.6	24.3

[a] Rate constants in 10^{-15} cm^3 molecule^{-1} s^{-1}. [b] Solvation time in fs. [c] Conventional transition state theory. [d] CVT/ZCT. [e] CVT/SCT. [f] CVT/μOMT.

Table 5. Speedup ($k_{Solution}/k_{Gas}$) of R1

level	τ^a	D_k	TST[b]	CVT	ZCT[c]	SCT[d]	μOMT[e]
SES			1.49	1.19	1.21	1.05	0.98
ESP	0	∞	1.96	2.73	2.41	1.99	2.01
NES	10	D_k^A	0.71	1.00	0.85	0.67	0.89
NES	10	$D_k^G/4$	0.10	0.16	0.14	0.11	0.32
NES	10	$D_k^G/2$	0.37	0.55	0.48	0.37	0.55
NES	10	D_k^G	0.80	1.14	0.99	0.78	0.96
NES	10	$2D_k^G$	1.22	1.72	1.50	1.21	1.37
NES	10	$4D_k^G$	1.54	2.15	1.88	1.55	1.64
NES	10	$8D_k^G$	1.74	2.42	2.11	1.74	1.79
NES	10	$16D_k^G$	1.85	2.56	2.25	1.85	1.87
NES	10	$20D_k^G$	1.88	2.60	2.28	1.87	1.88

[a] Solvation time in fs. [b] Conventional transition state theory. [c] CVT/ZCT. [d] CVT/SCT. [e] CVT/μOMT. We notice that in all cases the CVT/μOMT result, are within 2% the large-curvature[82] limit.

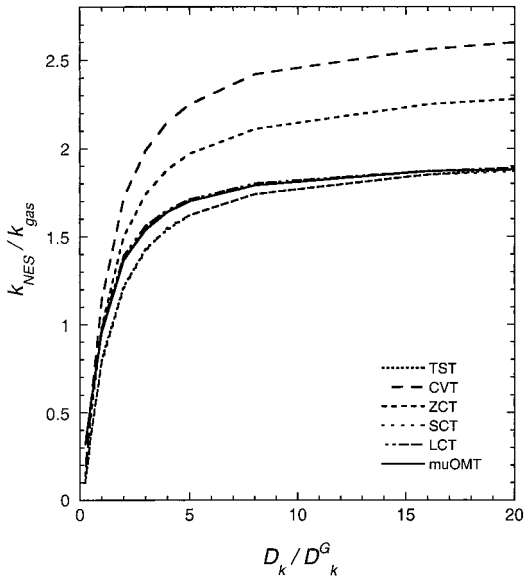

Figure 6. The ratio k_{NES}/k_{gas} as a function of the scaling of the atomic diffusion constants. All calculations for the figure were carried out with $\tau = 10$ fs.

level, 0.41 for CVT/ZCT, 0.39 for CVT/SCT, and 0.48 for CVT/μOMT. Tables 4 and 5 show that similar ratios for CVT and CVT/μOMT persist when D_k is large (weak solute−solvent coupling), but large-curvature tunneling begins to be effected differently from overbarrier reaction or small-curvature tunneling when the solute−solvent coupling increases. For example, when all effective atomic diffusion coefficients are divided by 4, the nonequilibrium effects are 0.054−0.058 the CVT, CVT/ZCT, and CVT/SCT levels, but 0.16 at the CVT/μOMT level. This is somewhat contrary to the lore of the field where nonequilibrium solvation effects are sometimes guessed to be larger when tunneling effects are larger.

Table 6. Kinetic Isotope Effects (k_{HH}/k_{DH}) at 298 K in Aqueous Solution[a]

level	τ^b	D_k	TST	CVT	ZCT[c]	SCT[d]	LCT[e]	μOMT[f]
SES			0.44	0.27	0.53	0.81	0.53	0.48
ESP	0	∞	0.39	0.34	0.60	0.91	0.51	0.51
NES	10	D_k^A	0.27	0.24	0.41	0.60	0.49	0.49
NES	10	$D_k^G/4$	0.17	0.17	0.27	0.39	0.25	0.25
NES	10	$D_k^G/2$	0.23	0.22	0.36	0.53	0.34	0.34
NES	10	D_k^G	0.29	0.26	0.44	0.66	0.37	0.37
NES	10	$2D_k^G$	0.33	0.29	0.50	0.76	0.42	0.42
NES	10	$4D_k^G$	0.35	0.31	0.53	0.80	0.44	0.44
NES	10	$8D_k^G$	0.36	0.32	0.55	0.84	0.44	0.44
NES	10	$16D_k^G$	0.37	0.33	0.56	0.85	0.46	0.46
NES	10	$20D_k^G$	0.38	0.34	0.58	0.87	0.49	0.50

[a] The experiemental KIE is 0.7, $k_{HH}/k_{DH} = k(H + CH_3OH)/k(D + CH_3OD)$. [b] Solvation time in fs. [c] CVT/ZCT. [d] CVT/SCT. [e] CVT/LCT. [f] CVT/μOMT.

Table 7. Kinetic Isotope Effects (k_{HH}/k_{HD}) at 298 K in Aqueous Solution[a]

level	τ^b	D_k	TST	CVT	ZCT[c]	SCT[d]	LCT[e]	μOMT[f]
SES			10.3	10.9	10.3	14.6	28.3	21.3
ESP	0	∞	10.3	10.7	9.50	13.3	26.6	20.2
NES	10	D_k^A	8.13	8.47	7.35	10.1	23.1	18.6
NES	10	$D_k^G/4$	6.19	6.93	6.11	8.42	17.9	16.8
NES	10	$D_k^G/2$	7.69	8.30	7.27	10.0	22.3	18.9
NES	10	D_k^G	8.77	9.23	8.18	11.3	24.2	19.5
NES	10	$2D_k^G$	9.45	9.84	8.69	12.2	25.7	20.2
NES	10	$4D_k^G$	9.76	10.1	8.92	12.5	25.8	20.1
NES	10	$8D_k^G$	9.95	10.3	9.10	12.7	25.8	20.1
NES	10	$16D_k^G$	10.1	10.4	9.21	13.0	25.9	19.9
NES	10	$20D_k^G$	10.2	10.6	9.36	13.0	26.0	19.8

[a] The experiemental KIE is 20, $k_{HH}/k_{HD} = k(H + CH_3OH)/k(H + CD_3OH)$. [b] Solvation time in fs. [c] CVT/ZCT. [d] CVT/SCT. [e] CVT/LCT. [f] CVT/μOMT.

Table 4 includes conventional transition state theory. The primary point to be made about those results is that they differ from our best results, again underscoring that conventional transition state theory does not provide reliable estimates of absolute rate constants.[85] From Figure 5, we notice that the ratio of the NES rate constant to the gas-phase rate constant increases as the diffusion constants increase. As mentioned above, the experimental value of this "speed up" was estimated to be 1.8 by us[3] and 1.2 by Mazyk and Bartels.[94] In Figure 5, we also notice that the inclusion of the large-curvature-tunneling contribution improves the calculated ratio.

It is interesting to consider two kinetic isotope effects (KIEs), namely, (i) $D + CH_3OD \rightarrow DH + CH_2OD$ and (ii) $H + CD_3OH \rightarrow HD + CD_2OH$. The corresponding KIEs are denoted as (i) k_{HH}/k_{DH} and (ii) k_{HH}/k_{HD}, where the first index means the attacking species and the second index means the transferred species. Table 6 gives the calculated KIEs for (i), and Table 7 gives the calculated KIEs for (ii). As the diffusion constants increase, the value of the KIE kinetic tends to the ESP limit due to a decrease in the coupling between the solvent and solute coordinates. The experimental estimation of the KIEs for (i) is 0.7 by Lossack et al.[95] and for (ii) is 20 by Anbar et al.[96]

(95) Lossack, A. M.; Roduner, E.; Bartels, D. M. *J. Phys. Chem.* A **1998**, *102*, 7462.

5. Concluding Remarks

Many recent advances in transition state theory have generated an appreciation of the role of nonequilibrium solvation and solvent friction on the rates of chemical reactions,[7,16] but so far there has been no framework for incorporating these effects into practical direct dynamics calculations of liquid-phase reactions. In this paper, we have presented a method for calculating nonequilibrium solvation effects on liquid solution rate constants by variational transition state theory with multidimensional tunneling (VTST/MT); the method is applicable even for large-curvature corner-cutting tunneling paths. The method is general from the point of view of the number of atoms and type of potential function for the solute and from the point of view of type of tunneling path, but it is limited to the linear response regime for solute−solvent coupling. We applied this treatment to a free radical reaction in aqueous solution that has previously been studied both experimentally[94−96] and theoretically.[3] In this treatment, the 3*N* solute Cartesian coordinates are coupled multilinearly to a collective solvent coordinate *y* based on the generalized Langevin equation. Unlike previous calculations in the literature (except ref 42), the collective solvent coordinate is coupled dynamically to all degrees of freedom of the solute. We use the Wilson ***GF*** matrix method with redundant internal coordinates to separate the vibrational and rotational motion of the solute. To calculate the coupling constants between the solvent and solute coordinates, it is required to estimate the solvation time and the effective atomic diffusion constants. Two schemes are proposed to approximate the atomic diffusion constants; one is based on the solvent-accessible surface area and the other is based on the free energy of solvation. The latter is a better justified approximation due to the nature of the solute−solvent long-range forces. The solvation time can be obtained from the velocity autocorrelation function generated from a molecular dynamics simulation or estimated based on the dipole moment, moments of inertia, density, dielectric constant, and temperature of the polar solvent. The ratio of the aqueous solution rate constant to the gas-phase rate constant depends on the solvation time and the effective atomic diffusion constants. We find that when the effective diffusion constants increase, the reaction rate tends to the no-coupling limit, which is equivalent to the equilibrium solvation path result. The kinetic isotope effects of R1 are also studied by using the same friction and diffusion parameters for the H and D atoms.

(96) Anbar, M.; Meyerstein, D. *J. Phys. Chem.* **1964**, *68*, 3184.

6. Summary

In the present work, we have presented a general linear-response method to treat nonequilibrium solvation effects that is applicable to polyatomic systems and can easily be extended to arbitrarily large solutes. We have used the new method to predict that nonequilibrium solvation is significant for a real bimolecular reaction of neutral species, in particular lowering the rate constants by a factor of 2 for H + CH_3OH. The calculations presented in this paper show generally good agreement with the experimental values, and they lead to insight into the factors affecting the magnitude of the nonequilibrium frictional effect.

Acknowledgment. The authors are grateful to Chris Cramer and Bruce Garrett for many helpful interactions. This work is supported in part by the National Science Foundation under Grant No. CHE97-25965.

JA991809I